Pakistan Veterinary Journal

ISSN: 0253-8318 (PRINT), 2074-7764 (ONLINE)
DOI: 10.29261/pakvetj/2025.261

RESEARCH ARTICLE

Nickel Exposure Via Different Routes Induces Hepato-Intestinal Injury and Conjugated Bile Acid Dysregulation in Mice

Shibin Yuan[1,2,3], Aifei Du[1], Yiwei Liu[1,4], Baolin Song[1,5,6], Shaohua Feng[1], Wei Luo[1], Chunjia Li[1], Xiaobao Ding[1], Shangqing Lu[1], Tingting Fang[1,2,3], Le Wang[1,2,3] and Bangyuan Wu[1,2,3*]

[1]College of Life Science, China West Normal University, Nanchong 637000, Sichuan, China; [2]Key Laboratory of Southwest China Wildlife Resources Conservation (Ministry of Education), Nanchong 637000, Sichuan, China; [3]Nanchong Key Laboratory of Wildlife Nutrition Ecology and Disease Control, Nanchong 637000, Sichuan, China; [4]Shanghai Veterinary Research Institute, Chinese Academy of Agricultural Sciences, Shanghai 201100, Shanghai, China; [5]Department of Infectious Diseases and Public Health, City university of Hong Kong, Kowloon, Hong Kong 999077, China; [6]Cornell Institute of Host-Microbe Interactions and Disease, Department of Entomology, Cornell University, Ithaca, New York State 14850, USA. [1]Aifei Du, Yiwei Liu, Baolin Song and Shibin Yuan contributed equally to this work.
*Corresponding author: wubangyuan2008@163.com; wby2008@cwnu.edu.cn

ARTICLE HISTORY (25-326)

Received: April 14, 2025
Revised: July 31, 2025
Accepted: August 07, 2025
Published online: October 07, 2025

Key words:
Bile acid transporters
Enterohepatic circulation
Environmental toxicology
Hepatic transcriptome
Nickel exposure

ABSTRACT

Nickel (Ni) ingestion is associated with hepatic and gastrointestinal toxicity, but its effects on bile acid metabolism and the role of exposure routes remain unclear. In this study, male mice were exposed to $NiCl_2$ (1.6mg/mL) via gavage or intraperitoneal injection for 28 days. Histological, ultrastructural, and immunohistochemical analyses were conducted on liver and intestinal tissues. Liver transcriptome sequencing and fecal bile acid profiling (via LC-MS/MS) were performed. Nickel exposure caused significant intestinal and liver damage, with intraperitoneal injections producing more severe effects than gavage. TUNEL and PCNA staining revealed increased apoptosis and reduced cell proliferation in the liver. Transmission electron microscopy showed mitochondrial swelling and cristae loss. Bile acid profiling indicated reduced secretion of bile acids, particularly conjugated bile acids. Transcriptomic analysis identified altered expression in bile acid transport and cholesterol metabolism genes, including down regulation of Abcb11, Slc22a7, and Aqp8. The result of this experiment confirmed that nickel could induce hepato-intestinal toxicity and disrupt bile acid metabolism in a route-dependent manner. These findings provide new insights into heavy metal toxicity and bile acid regulation.

To Cite This Article: Yuan S, Du A, Liu Y, Song B, Feng S, Luo W, Li C, Ding X, Lu S, Fang T, Wang L and Wu B 2025. Nickel exposure via different routes induces hepato-intestinal injury and conjugated bile acid dysregulation in mice. Pak Vet J. http://dx.doi.org/10.29261/pakvetj/2025.261

INTRODUCTION

Nickel is essential in producing many industrial materials, electronic components, and aerospace alloys, and is considered a widespread environmental pollutant (Arita *et al.*, 2012; Song *et al.*, 2017). In recent decades, excessive industrial and agricultural discharge has led to the accumulation of nickel in soil, water, and vegetation (Changyuan, 2015; Dai *et al.*, 2016). Both humans and animals can be exposed to nickel through contaminated drinking water, feedstuffs, or forage plants, as well as through inhalation and dermal absorption from the polluted environments (Kaphle *et al.*, 2024). In rural or agricultural regions such as Sichuan, China, animals may be at a particular risk due to increased exposure to polluted water sources and industrial runoff.

Nickel exposure has been associated with adverse effects on growth, immunity, and gastrointestinal function in animals. In livestock and experimental models, histopathological damage has been reported in the liver and intestines, including hepatocellular degeneration, sinusoidal congestion, villus atrophy, and epithelial erosion (Cempel and Janicka, 2002; Sidhu *et al.*, 2005; Wu *et al.*, 2013a; Wu *et al.*, 2014). In humans, acute or chronic exposure can cause gastrointestinal symptoms such as vomiting, diarrhea, and abdominal pain (Zou *et al.*, 2017; Guo *et al.*, 2019). Despite this, studies have largely focused on oxidative stress, inflammation, or general tissue injury, with limited attention paid to the effects of nickel on bile acid metabolism, an essential hepatic function directly linked to intestinal health (Di Ciaula *et al.*, 2017).

Bile acids, synthesized in the liver and secreted into the intestine, are critical for lipid digestion and are continuously recycled through enterohepatic circulation. Disruption of bile acid synthesis or transport can reflect hepatic dysfunction and compromise gut-liver communication (Ringseis *et al.*, 2020). Since the route of toxicant administration can significantly alter organ exposure and systemic response (Das *et al.*, 2008), understanding how nickel affects liver–intestinal physiology via different exposure routes is essential. However, the mechanisms by which nickel influences bile acid metabolism especially conjugated bile acids and its associated transcriptomic changes, remain largely unclear.

Therefore, in this study, we investigated the toxicological effects of nickel exposure on the liver and intestine in mice, comparing two common exposure routes: oral gavage and intraperitoneal injection. By integrating histopathology, ultrastructure, transcriptomics, and bile acid profiling, we aimed to elucidate the mechanism of nickel-induced liver–gut injury and bile acid dysregulation. Although laboratory mice were used, the findings are also of relevance to veterinary toxicology, as livestock in agricultural or industrial areas may be exposed to nickel through contaminated water, forage, or soil.

MATERIALS AND METHODS

Experimental animals and grouping: One hundred 4-week-old male Kunming mice (Experimental Animal Center, North Sichuan Medical College, Sichuan, China) with an initial weight of 24.02±1.12g were randomly divided into four groups: gavage nickel group (GN), gavage normal saline group (GNS), intraperitoneal injection of nickel group (IN) and intraperitoneal injection of normal saline group (INS), with five replicates in each group. All animals were housed in compliance with guidelines under controlled environmental conditions (temperature: 24±2°C; humidity: 55±5%). Dietary and hydration needs were met through the continuous availability of a certified rodent maintenance diet and pure water. Experimental manipulations were conducted as follows: GN/GNS group: oral administration via gavage with either 1.6mg/mL $NiCl_2$ solution (Wu *et al.,* 2022a) or saline; IN/INS groups: equivalent dosing via intraperitoneal injection using identical solution concentrations (Wu *et al.,* 2022). The group and treatment methods are shown in Table 1. Among them, the GNS group was the blank control group for the GN group, and the INS group was the blank control group for the IN group. All groups were treated for 28 days.

Table 1: Mice grouping and administration methods

Group	Exposure model	Treatment
GN	Gavage	0.25ml $NiCl_2$ (1.6mg/ml)
GNS	Gavage	0.25ml normal saline
IN	Intraperitoneal injection	0.25ml $NiCl_2$ (1.6mg/ml)
INS	Intraperitoneal injection	0.25ml normal saline

Organ coefficient determination: Following humane euthanasia, animals were immediately placed on a refrigerated surgical platform (4°C) for necropsy. Organ harvest was conducted under sterile conditions, with each organ system meticulously excised and cleared of residual blood via saline perfusion. Post-excision, organs were subjected to gravimetric analysis using calibrated electronic scales, with organometallic indices calculated according to the standardized formula:

$$\text{Organ Index} = \text{Organ Mass} / \text{Body Mass}$$

Observation of pathological changes in intestinal and hepatic cells: The intestinal and liver tissue samples were fixed with 4% paraformaldehyde after dissection. Then, they were dehydrated with 75%, 85%, 95%, 100%I, and 100%II gradient alcohol for 4h, 2h, 2h, 1h, and 30min, respectively. Dehydrated tissue was treated with xylene to make it transparent. The transparent tissue was immersed in melted paraffin for 2h so that the paraffin could completely replace the transparent agent in the tissue. Then, the thickness regulator of the microtome was adjusted to a thickness of 5μm for sectioning, followed by water bath-assisted section flattening. For staining purposes, standard H&E staining protocols were applied. Microscopy was employed for histologic examination of liver and intestinal sections. Quantitative morphometric analysis was conducted using ViewPoint software, measuring parameters including intestinal villus height; crypt depth; and mucosal layer thickness.

TUNEL cell apoptosis and PCNA cell proliferation assay: The liver paraffin sections were stained according to the instructions of the TUNEL cell apoptosis detection kit (DAB chromogenic method) (Cat. No.: C1091, purchased from Beyotime Biotech. Inc.) and the PCNA cell proliferation detection kit (IHC) (Cat.No.:E607250, purchased from Sangon Biotech. Inc.) and then photographed under a light microscope.

Transmission electron microscopy: Cubic liver specimens ($1mm^3$) underwent primary fixation in 2.5% glutaraldehyde followed by secondary fixation in 2% osmium tetroxide buffered with veronal acetate. Dehydration proceeded through ascending ethanol series (50-100%) before infiltration and embedding in araldite. Ultrathin sections were obtained using an ultramicrotome, mounted on 200-mesh copper grids, and double-stained with uranyl acetate and lead citrate. Samples were visualized using a JEOL JEM-1400 transmission electron microscope operated.

Transcriptomic analysis of changes in hepatocyte signaling pathways: Liver tissue samples were subjected to transcriptome sequencing analysis. First, the total RNA of each group was extracted by the magnetic bead method, and mRNA containing polyA structure was enriched by oligo(dT) magnetic beads. RNA was randomly fragmented into approximately 300bp fragments, and random hexamer primers were used to guide reverse transcription for the synthesis of single-stranded cDNAs, which were then used as templates for the synthesis of double-stranded cDNAs, then used it as a template for double-stranded cDNA synthesis. After completing the steps of library construction, such as end repair and junction ligation, the library was enriched by PCR amplification, and the target fragments of about 450 bp were screened by gel electrophoresis. An Agilent-2100 Bioanalyzer was used to perform library quality control and quantify the total

concentration and effective concentration of the library. According to the requirement of sequencing data volume, the libraries containing specific Index tags were mixed proportionally (each sample was set with an independent Index for subsequent data splitting), and 2nM standard libraries were prepared. After single-stranded DNA was obtained by alkaline denaturation, double-end sequencing was performed on the Illumina sequencing platform. The raw sequencing data were filtered by quality control to obtain high-quality clean data. The gene expression profiles were determined by genomic comparison, and then bioinformatics analysis, such as differential expression analysis, functional enrichment analysis, and clustering analysis, was carried out.

Analysis of bile acid secretion: Fecal specimens from mice in each experimental group were collected and processed with ice-cold methanol at a 6μL:1mg (methanol: fecal aliquot) ratio. The samples were homogenized by grinding, followed by 1-min vigorous vortex mixing and 30-min sonication at 4°C. After centrifugation at 12,000rpm for 10min, the pellet underwent two consecutive extraction cycles using the same methanol-based protocol (vertexing, sonication, centrifugation). Supernatants from both extractions were pooled and evaporated to dryness. The extracts were redissolved in 200μL of methanol (containing internal standard 50ng/mL), centrifuged for 15min, and the supernatant was used for machine detection. MRM parameters were obtained, integrated by MultiQuant software and bile acid content was calculated according to the internal standard one-point method. The results of principal component analysis (PCA), OPLS-DA analysis, and differential component analysis were further examined. Then, principal component analysis and difference analysis were performed.

Statistical analysis: Statistical analyses were conducted with SPSS software (version 26.0), with quantitative data expressed as mean±standard deviation. Intergroup comparisons were assessed by one-way ANOVA, followed by the least significant difference (LSD) post hoc test for pairwise analyses. Statistical significance thresholds were defined as $P<0.05$ for all comparisons.

RESULTS

Effect of nickel on growth performance: As shown in Table 2, nickel injection decreased the final body weight and average daily gain of the mice ($P<0.01$). Nickel gavaging decreased average daily food intake significantly ($P<0.01$).

Table 2: Growth performance of mice

Group	Initial weight	Final weight	Total weight gain	Average daily gain	Average daily feed intake
GN	24.08 ± 1.59^{a}	31.64 ± 0.95^{b}	7.55 ± 1.10^{bAB}	0.30 ± 0.04^{bAB}	6.24 ± 0.18^{bB}
GNS	24.24 ± 0.55^{a}	33.59 ± 1.92^{b}	9.35 ± 1.38^{abAB}	0.37 ± 0.06^{abAB}	8.47 ± 0.47^{aA}
IN	24.21 ± 0.75^{a}	31.15 ± 1.61^{b}	6.94 ± 1.26^{bB}	0.28 ± 0.05^{bB}	6.13 ± 0.99^{bB}
INS	23.55 ± 1.57^{a}	35.21 ± 1.37^{a}	11.65 ± 2.12^{aA}	0.47 ± 0.08^{aA}	7.55 ± 0.76^{aAB}

Effect of nickel on organ coefficients and intestinal morphology: Nickel exposure resulted in significant changes in organ coefficients and intestinal structure. As shown in Fig. 1A, the liver coefficient was significantly increased in the IN group compared to INS ($P<0.05$), while colon and cecum coefficients were significantly reduced in both GN and IN groups relative to controls ($P<0.05$). Coefficients of the small intestine segments (duodenum, jejunum, ileum) showed no significant differences.

Histological analysis revealed notable differences in intestinal morphology among groups (Fig. 1B). The GN and IN groups showed shortening, fragmentation, and structural loss of intestinal villi. Quantitative measurements indicated significant reductions in villus height across all intestinal segments in both GN and IN groups (Fig. 1C), along with decreased crypt depth (Fig. 1D) and V/C ratio (Fig. 1E), particularly in the duodenum and ileum.

Further analysis showed that villus width (Fig. 1F), villus area (Fig. 1G), and mucosal/muscular thickness (Fig. 1H) were all significantly decreased in the GN and IN groups compared to respective controls ($P<0.05$).

Nickel induces liver transcriptomic changes: Principal component analysis (PCA) revealed distinct clustering of gene expression profiles among the four treatment groups (Fig. 2A), indicating that nickel exposure markedly altered hepatic transcriptomes. Volcano plots showed that 802 differentially expressed genes (DEGs) were identified in the GN vs. GNS comparison (224 upregulated, 558 downregulated), and 773 DEGs in the IN vs. INS comparison (421 upregulated, 352 downregulated) (Fig. 2B-a, 3C-a). Heatmaps demonstrated strong intra-group consistency and separation between treatments and controls (Fig. 2B-b, 3C-b).

GO enrichment analysis revealed that DEGs in the GN group were mainly associated with extracellular structure organization and tissue development, whereas those in the IN group were enriched in metabolic processes and immune-related responses (Fig. 2C-c, 2C-d, 2C-e, 2C-f). KEGG pathway enrichment further indicated that nickel gavage primarily affected ECM–receptor interaction and bile secretion pathways, while intraperitoneal injection influenced cholesterol metabolism, galactose metabolism, and retinol metabolism (Fig. 2B-c–f).

Effect of nickel on the liver morphology, apoptosis, proliferation, and ultrastructure: To explore the damaging effect of nickel on the liver, H&E staining, TUNEL staining, and PCNA staining methods were used to observe their pathological changes, cell apoptosis, and cell proliferation of the liver tissue, as shown in Fig. 3. The hepatocytes in the INS and GNS groups were orderly arranged having uniform size with round nuclei, and there were no large numbers of red blood cells in the central veins or hepatic sinusoids (Fig. 3A). In the GN and IN group, the liver cells were arranged disorderly. The cells were swollen, the hepatic sinusoids became narrow or even disappeared, the nuclei showed pyknosis with variable sizes, and many red blood cells were filled in the central vein and hepatic sinusoids (Fig. 3A). In the IN group, there were vacuoles in the cells with severe lesions (Fig. 3A). In the GN and IN groups, there were more positive cells than in the GNS and INS groups under TUNEL staining. It shows nickel-induced hepatocyte apoptosis (Fig. 3B). In addition, PCNA staining results showed fewer positive

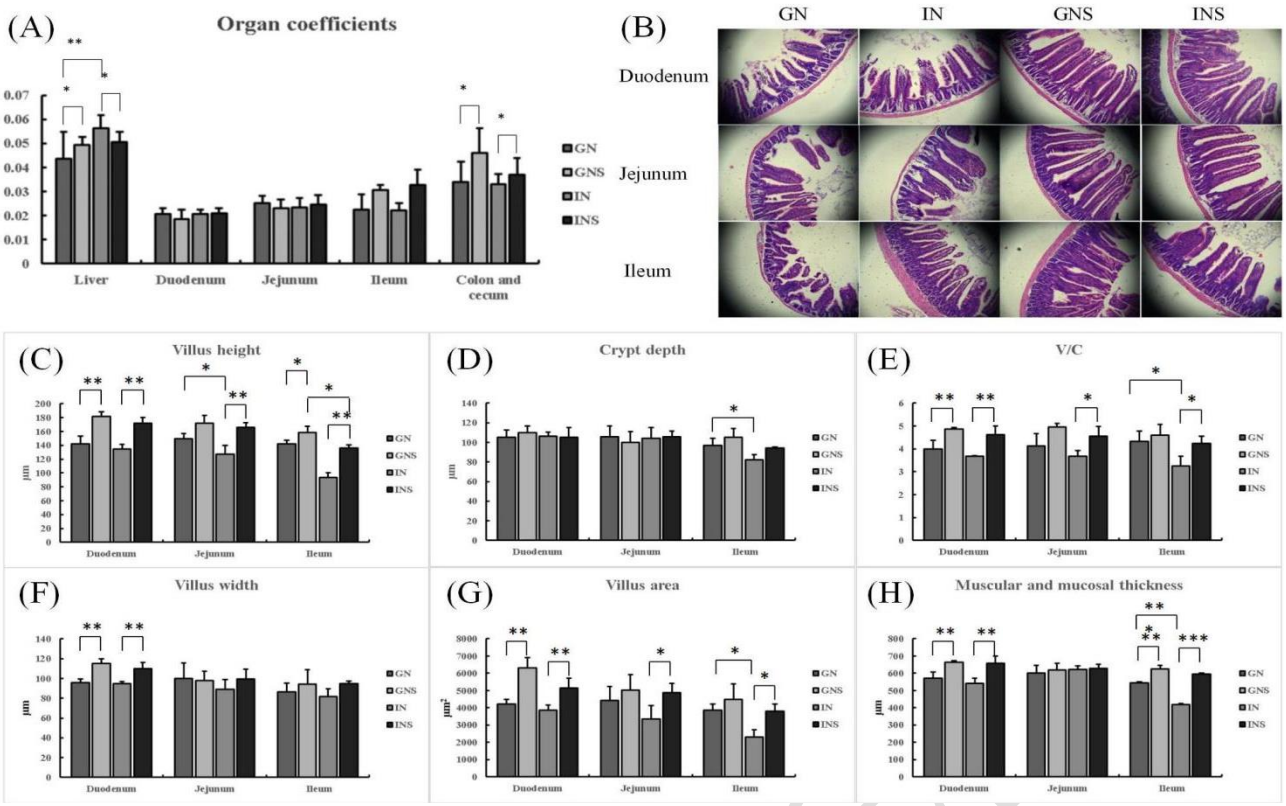

Fig. 1: Effects of nickel exposure on organ coefficients and intestinal morphology. (A) Organ coefficients of liver, duodenum, jejunum, ileum, and colon + cecum. (B) H&E-stained sections of duodenum, jejunum, and ileum in each group (GN: gavage nickel; IN: injection nickel; GNS/INS: saline controls). (C) Villus height; (D) Crypt depth; (E) Villus height/crypt depth ratio (V/C); (F) Villus width; (G) Villus area; (H) Thickness of mucosa and muscularis. All data are presented as mean±SEM. *P<0.05, **P<0.01, ***P<0.001 indicate statistically significant differences between groups.

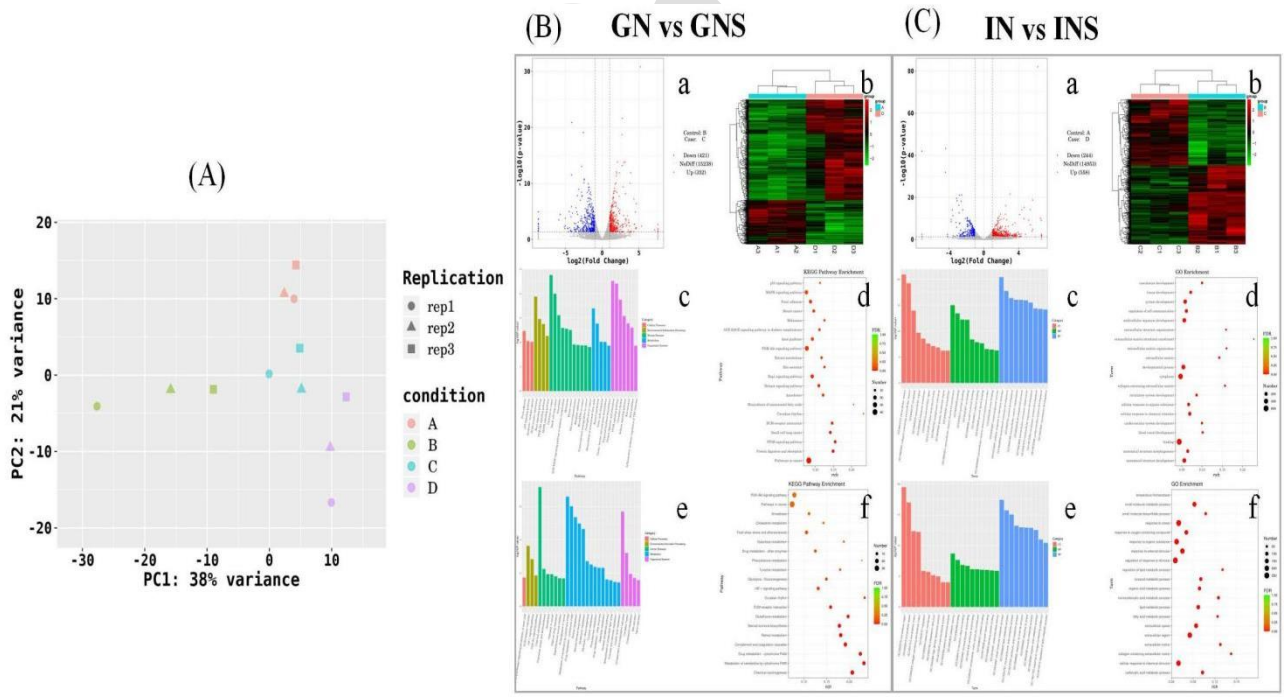

Fig. 2: Transcriptomic profiling of mouse liver following nickel exposure. (A) PCA plot showing separation among groups based on liver gene expression profiles. (B) Differential expression analysis in GN vs. GNS groups: (a) Volcano plot of DEGs; (b) Heatmap of gene expression; (c, d) GO enrichment (bar and bubble charts); (e, f) KEGG pathway enrichment. (C) Differential expression analysis in IN vs. INS groups: (a) Volcano plot; (b) Heatmap; (c, d) GO enrichment; (e, f) KEGG enrichment. DEGs were defined as P<0.05 and fold change > 2.

cells in the GN and IN groups, suggesting that nickel inhibited hepatocyte proliferation (Fig. 3C). In GN and IN groups, swollen mitochondria and disrupted or disappeared cristae were observed in hepatocytes, and the changes were more serious in the IN group than in the GN group. In contrast, the mitochondria in the INS and GNS groups showed more complete structures and morphologies (Fig. 3D).

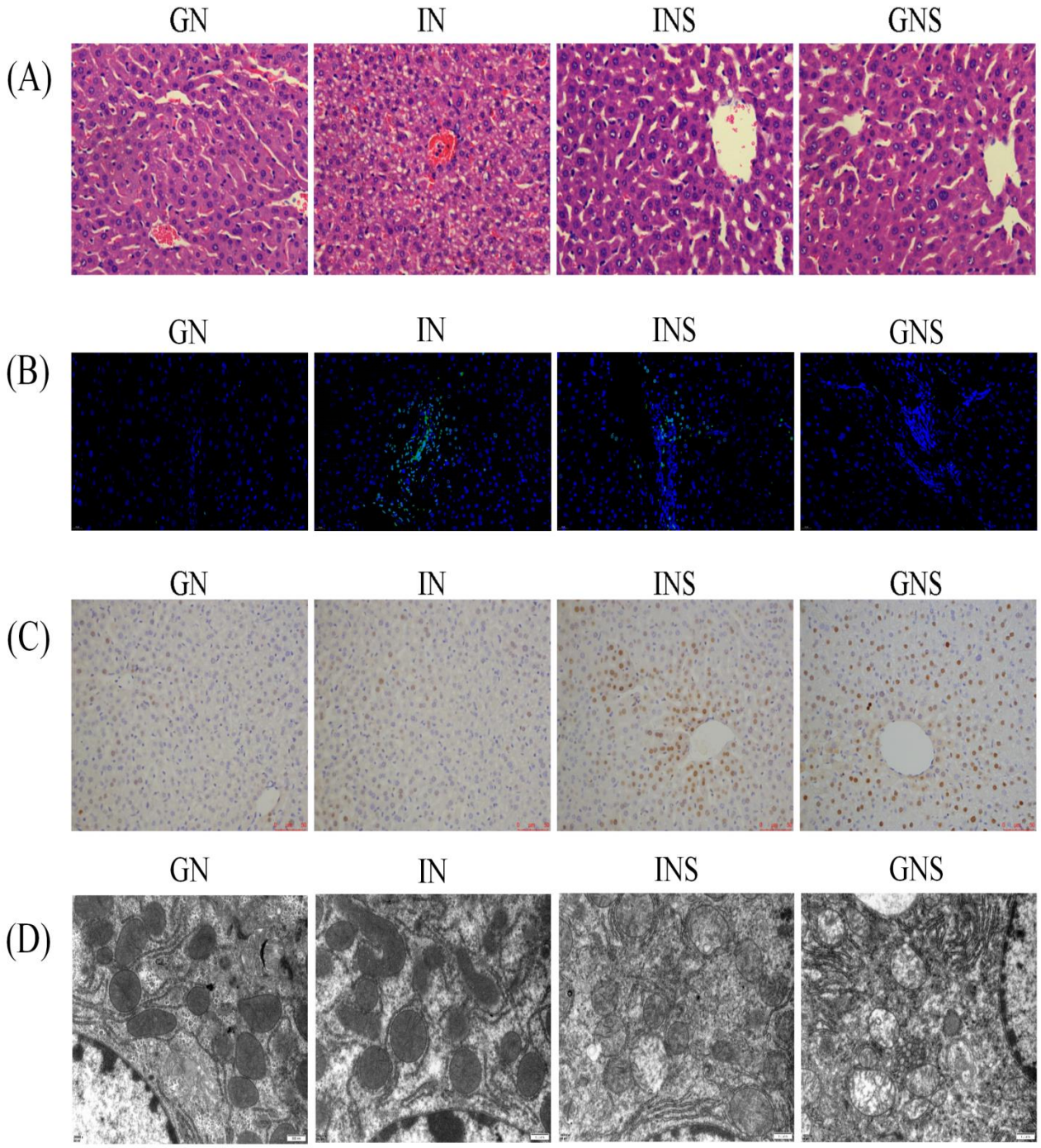

Fig. 3: Effects of nickel on mouse liver: (A) H&E staining of liver tissue; (B) TUNEL staining of liver tissue; (C) PCNA staining in liver tissue; (D) Ultrastructural changes in hepatocytes.

Nickel induces changes in the liver transcriptomics: Multivariate analysis of fecal bile acid profiles revealed significant differences between groups. PCA and biplot analyses showed that bile acid composition differed markedly between Ni-treated and control groups, with clear group separation (Fig. 4A–B). OPLS-DA score plots further confirmed this separation for both GN vs. GNS and IN vs. INS comparisons (Fig. 4C–D). Model quality was verified with high R^2 and Q^2 values (Fig. 4E–F).

Volcano plots (Fig. 4G–H) and VIP analysis (Fig. 4I–J) identified significantly altered bile acids in both GN and IN groups. Heatmaps showed consistent group-level clustering and bile acid suppression (Fig. 4K–L).

Differential expression of bile secretion and cholesterol metabolism genes: In transcriptomic comparisons between the GN and GNS groups, differentially expressed genes associated with bile secretion were identified (Fig. 5A). The analysis revealed 3 upregulated and 7 downregulated transcripts in the GN group relative to the GNS group. Similarly, the evaluation of cholesterol metabolism pathways in the IN versus INS comparison demonstrated transcriptional alterations, with 5 genes showing increased expression and 2 genes exhibiting reduced expression in the IN group (Fig. 5B). These pathway-specific modulations reflected distinct regulatory mechanisms under experimental conditions.

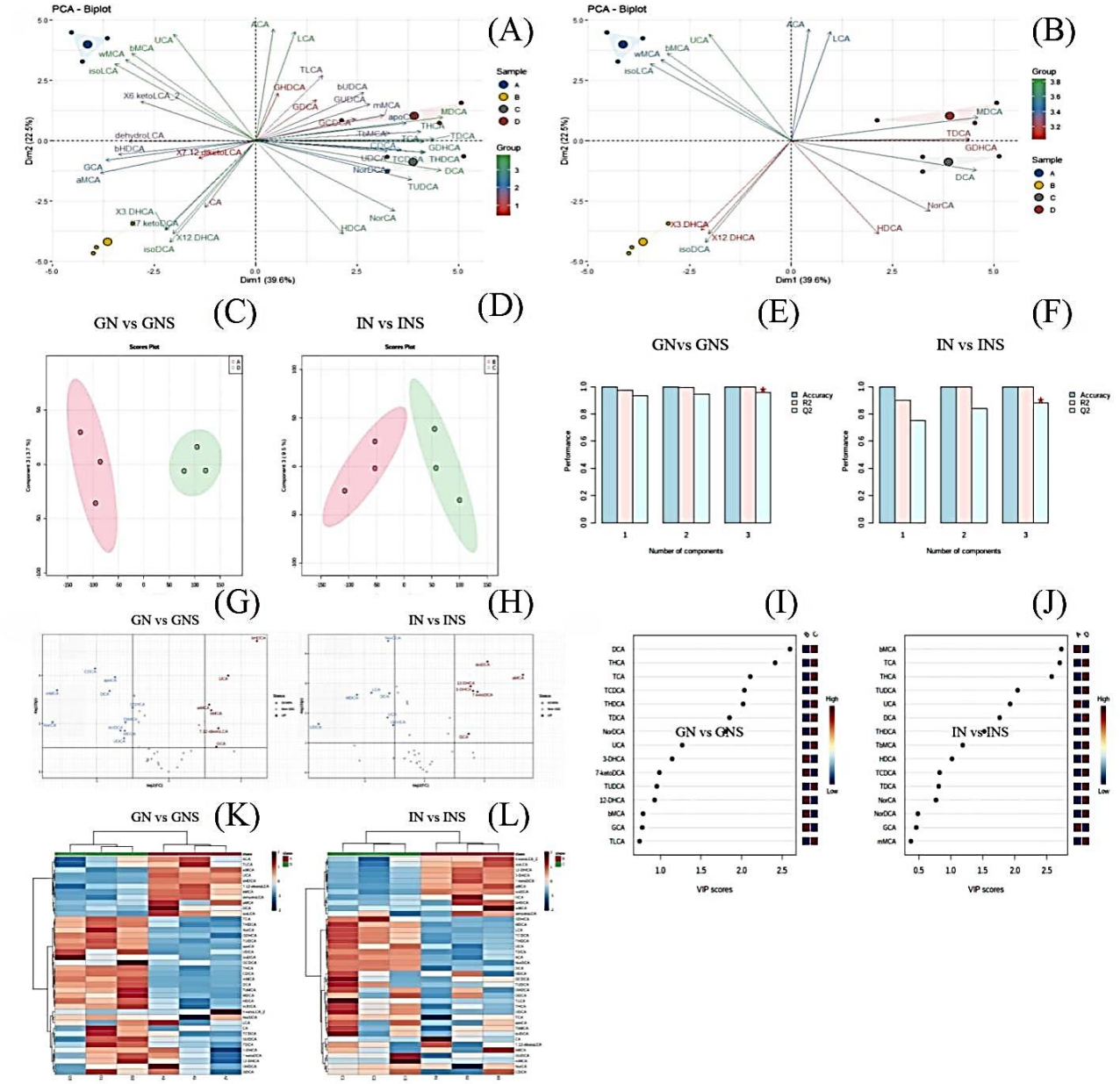

Fig. 4: Bile acid metabolomic alterations induced by nickel exposure. (A–B) PCA-biplot analysis of bile acid composition in fecal samples, showing group separation. (C–D) OPLS-DA score plots comparing GN vs. GNS (C) and IN vs. INS (D). (E–F) OPLS-DA model performance metrics (R^2, Q^2). (G–H) Volcano plots of differentially expressed bile acids. (I–J) VIP scores for top bile acid contributors to group separation. (K–L) Heatmaps of bile acid levels in GN vs. GNS and IN vs. INS.

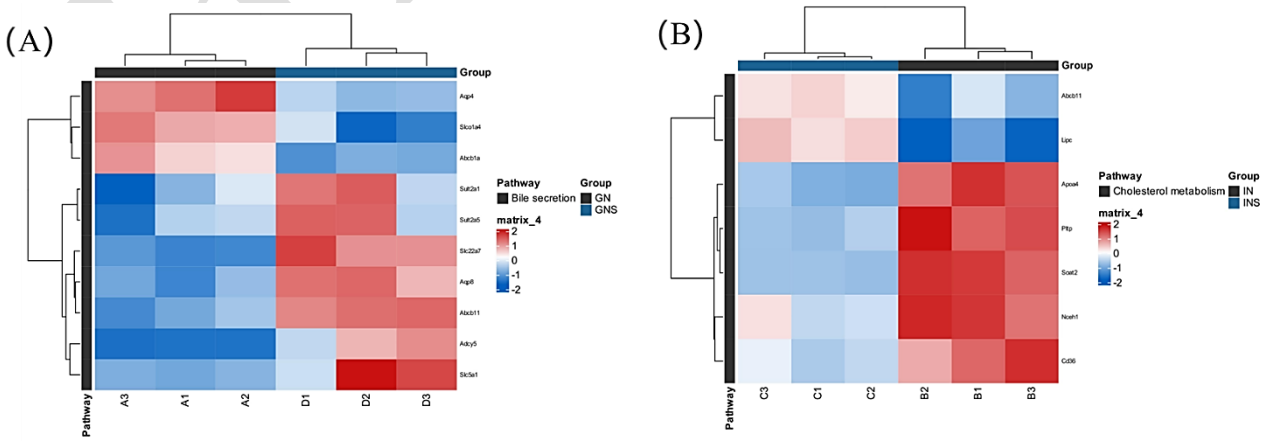

Fig 5: Heat map of differential expression of bile secretion and cholesterol metabolism genes. (Red indicates highly expressed genes, blue indicates low expressed genes): (A) Differential expression of bile secretion genes; (B) Differential expression of cholesterol metabolism genes.

DISCUSSION

Nickel ingestion has been associated with a wide spectrum of hepatic and gastrointestinal disorders. Studies have shown that Ni exposure can trigger oxidative stress, hepatocyte apoptosis, and lipid metabolic disturbances in the liver and intestine (Wu *et al.,* 2013b; Guo *et al.,* 2016a; Abudayyak *et al.,* 2020). However, relatively few studies have investigated how Ni could affect bile secretion, particularly in relation to coordinated organ- and transcriptome-level changes. Our study focuses on the liver–intestine axis, emphasizing bile acid synthesis, transport, and the systemic consequences of exposure via different administration routes.

Nickel exposure significantly impaired growth performance in mice, with both gavage (GN) and intraperitoneal injection (IN) groups showing reduced body weight, being consistent with previous findings in rabbits and broilers (Arpasova *et al.,* 2007; Bersényi *et al.,* 2008). Decreased feed intake may partly explain this effect, as nutrient availability and energy metabolism are closely tied to gastrointestinal function (Winter, 2006).

Nickel ingestion has been linked to gastrointestinal symptoms such as nausea, diarrhea, and abdominal pain. Consistent with this, our data showed decreased organ coefficients of the colon and cecum, particularly in the GN group. This reduction may be attributable to disrupted bile acid excretion, which may compromise the intestinal barrier and digestive capacity (Ringseis *et al.,* 2020). H&E staining revealed significant structural compromise in the intestinal villi, especially reduced villus height, crypt depth, and muscularis thickness. The GN group exhibited localized injury to the duodenum and ileum, whereas the IN group showed broader intestinal damage, suggesting route-dependent differences in gut toxicity. These findings align with prior studies on other metals such as cadmium and arsenic, which also impair intestinal architecture and absorption (Jiang *et al.,* 2020; Zhou *et al.,* 2025). The route-dependent injury pattern may result from differences in first-pass metabolism. IN exposure bypasses the gut and directly enters systemic circulation, likely concentrating Ni in the liver. This is consistent with our observation of more severe hepatic lesions in the IN group. By contrast, gavage exposes the intestinal epithelium directly, contributing to localized injury. This spatial distribution suggests complex hepato-intestinal interactions and involvement of bile acid-mediated signaling. The enterohepatic cycle, comprising bile secretion, intestinal absorption, and hepatic reuptake is especially susceptible to toxicant interference (Chiang, 2013).

Our data showed that Ni exposure severely damaged the liver, particularly in the IN group, with increased apoptosis, reduced proliferation, and disrupted mitochondrial ultrastructure. Transcriptomic analysis indicated that GN-induced DEGs were enriched in extracellular matrix (ECM)-related functions, while IN-induced DEGs were enriched in metabolism, immune signaling, and lipid pathways. ECM remodeling is critical for maintaining hepatic architecture and cellular interactions (Hynes, 2009), whereas dysregulated metabolism is frequently associated with hepatic steatosis and toxicity (Li *et al.,* 2021).

Notably, KEGG pathway analysis revealed significant activation of the PI3K-Akt pathway, a central modulator of apoptosis, cell survival, and metabolism. Mitochondrial damage and cytochrome release further confirmed apoptotic activation via intrinsic pathways (Naryzhnaya *et al.,* 2019). These molecular findings are consistent with earlier toxicological models of metal-induced hepatotoxicity (Tammam *et al.,* 2022; Guo *et al.,* 2023). Additionally, our study uncovered a striking reduction in conjugated bile acids in both GN and IN groups, measured via HPLC-MS, indicating a systemic disruption in bile acid synthesis and transport. This finding is consistent with previous work on other toxins such as deoxynivalenol and nickel nanoparticles, which reduce bile acid levels and suppress related enzymes (Zhang *et al.,* 2021; Wang *et al.,* 2022). Transcriptomic results revealed that GN exposure downregulated bile secretion genes (Slc22a7, Abcb11, Aqp8), while IN exposure upregulated cholesterol metabolism-related genes (SOAT, PLTP, NCEH1), which may contribute to intracellular fat accumulation and hepatocyte dysfunction (Sato, 2020).

These differences highlight that while GN primarily disrupts membrane transporters related to bile acid excretion, IN exposure primarily affects hepatocyte metabolism and cholesterol esterification. The shared downregulation of Abcb11, which encodes BSEP (a transporter of conjugated bile acids), offers a mechanistic link to the observed reduction in fecal bile acid output.

Our results thus support a dual-mode model of nickel-induced liver–gut toxicity: one where route-specific exposure leads to either transporter dysfunction (GN) or metabolic disruption (IN), ultimately converging on impaired enterohepatic circulation. These disruptions may be compounded by potential Ni-induced alterations in gut microbiota, which are required for conjugated bile acid biosynthesis (Wu *et al.,* 2022a).

The observed hepatointestinal injuries are not only mechanistically distinct but also biologically relevant to veterinary contexts. Chronic impairment of nutrient absorption, bile metabolism, and detoxification capacity can reduce feed conversion efficiency, increase susceptibility to infection, and compromise production in livestock raised under nickel-contaminated environments. Similarities in bile acid signaling and metabolism across mammalian species suggest these findings are broadly translatable to farm animals.

Our findings regarding nickel-induced damage to the liver and intestines, alongside altered bile acid secretion, are broadly consistent with prior studies but also introduce novel mechanistic insights. Several studies have demonstrated that chronic nickel exposure damages intestinal morphology, including reduced crypt depth and mucus production, thereby compromising intestinal function and barrier integrity. This aligns with our observations of decreased villus height, crypt depth, and epithelial integrity (Huang *et al.,* 2022; Feezan *et al.,* 2024). Nickel has also been implicated in hepatic dysfunction through pathways involving oxidative stress, mitochondrial disruption, and metabolic imbalance. Similar to their results, we observed hepatocyte apoptosis, disrupted proliferation, and mitochondrial cristae disappearance, particularly following intraperitoneal injection. Importantly, our data show for the first time that

nickel exposure significantly reduces the secretion of conjugated bile acids, especially via downregulation of key transporter genes like Abcb11 and Slc22a7. This complements findings from a metabolomics-based study that reported nickel nanoparticle exposure in rats reduced levels of bile acids such as cholic acid and deoxycholic acid and altered bile acid-related enzymes like CYP7A1 and SULT2A1 (Zhang *et al.,* 2021). Additionally, the decrease in conjugated bile acids may be partially attributed to nickel-induced damage in bile acid recycling and intestinal absorption pathways. Other studies have shown that toxins like deoxynivalenol and other mycotoxins can inhibit the expression of intestinal bile acid transporters (ASBT, IBABP, OSTα), leading to reduced reabsorption of conjugated bile acids (Wang *et al.,* 2022) We speculate that nickel may exert similar effects, disrupting the enterohepatic circulation and compounding hepatotoxicity.

Conclusions: This study demonstrates that nickel exposure causes significant hepato-intestinal toxicity in mice, with intraperitoneal injections inducing more severe damage than oral gavage. The observed intestinal villi atrophy, hepatic apoptosis, and mitochondrial degeneration were accompanied by decreased bile acid secretion, particularly conjugated bile acids. Transcriptomic analysis revealed distinct gene expression alterations associated with bile acid transport and cholesterol metabolism, including Slc22a7, Abcb11, Aqp8, SOAT, PLTP, and NCEH1. These findings suggest that nickel disrupts the hepato-enteric circulation and impairs liver detoxification and metabolic homeostasis. Our work highlights the importance of considering exposure routes in nickel toxicology and provides novel insights into the mechanisms underlying bile acid dysregulation. Future studies should further explore the interaction between nickel, bile acid transport, and gut-liver axis function.

CRediT authorship contribution statement: Shibin Yuan: Writing–original draft, Formal Analysis, Resources. Aifei Du: Writing–original draft, Validation, Investigation. Yiwei Liu: Methodology, Software, Formal Analysis. Shaohua Feng: Methodology, Software, Formal Analysis. Baolin Song: Software, Formal Analysis. Wei Luo: Validation, Investigation. Chunjia Li: Data Curation. Xiaobao Ding: Data Curation. Shangqing Lu: Investigation. Tingting Fang: Resources. Le Wang: Resources. Bangyuan Wu: Conceptualization, Formal Analysis, Supervision, Resources.

Funding: This study was fully supported by the Fundamental Research Funds of China West Normal University (Project No. 20A003), the Nanchong Key Laboratory of Wildlife Nutrition Ecology and Disease Control, Sichuan, China (NCKL202201) and the National Natural Science Foundation of China (32370557).

Declaration of Competing Interest: There is no known compete of interest to this study.

Ethical Statement: All animal experiments were approved by the Animal Welfare Committee of China West Normal University in accordance with the Laboratory Animal Guidelines for Ethical Review of Animal Welfare (China, cwnu2022D008).

Data availability: The data is available upon request to the Corresponding author.

Acknowledgement: In addition to the authors listed in this study, co-workers at China West Normal University helped conduct this study and monitor the experimental process. We would like to thank them for their contribution.

REFERENCES

Abudayyak. M, GÜzel. E, Özhan. G, 2020. Cytotoxic, Genotoxic, and Apoptotic Effects of Nickel Oxide Nanoparticles in Intestinal Epithelial Cells. Turk J Pharm Sci 17(4): 446-451.

Arita A, Niu J, Qu Q, *et al.*, 2012. Global levels of histone modifications in peripheral blood mononuclear cells of subjects with exposure to nickel. Environ Health Perspect 120(2): 198-203.

Arpasova H, Capcarova M, Kalafova A, *et al.*, 2007. Nickel induced alteration of hen body weight, egg production and egg quality after an experimental peroral administration. J Environ Sci Health B 42(8): 913-8.

Bersényi A, Berta E, Kádár I, *et al.*, 2008. Effects of high dietary molybdenum in rabbits. Acta Vet Hung 56(1): 41-55.

Cempel M and Janicka K, 2002. Distribution of nickel, zinc, and copper in rat organs after oral administration of nickel (II) chloride. Biol Trace Elem Res 90(1-3): 215-226.

Chiang JY, 2013. Bile acid metabolism and signaling. Compr Physiol 3(3): 1191-212.

Dai L, Koutrakis P, Coull BA, *et al.*, 2016. Use of the adaptive LASSO method to identify PM2.5 components associated with blood pressure in elderly men: The Veterans Affairs Normative Aging Study. Environ Health Perspect 124(1): 120-5.

Das KK, Das SN, Dhundasi SA, 2008. Nickel, its adverse health effects & oxidative stress. Indian J Med Res 128(4): 412-25.

Di Ciaula A, Garruti G, Lunardi Baccetto R, *et al.*, 2017. Bile Acid Physiology. Ann Hepatol 16(Suppl. 1: s3-105.): s4-s14.

Feezan A, Afzal S, Shoaib SM, *et al.*, 2024. Biochemical Impact of Nickel-Induced Metabolic impairment and the protective effects of resveratrol and ascorbic acid. J Food Biochem 2024(1): 8607956.

Guo H, Cui H, Fang J, *et al.*, 2016a. Nickel chloride (NiCl2) in hepatic toxicity: apoptosis, G2/M cell cycle arrest and inflammatory response. Aging (Albany NY) 8(11): 3009-3027.

Guo H, Liu H, Wu H, *et al.*, 2019. Nickel carcinogenesis mechanism: DNA damage. Int J Mol Sci 20(19):

Guo H, Wei L, Wang Y, *et al.*, 2023. Nickel induces hepatotoxicity by mitochondrial biogenesis, mitochondrial dynamics, and mitophagy dysfunction. Environ Toxicol 38(5): 1185-1195.

Huang L, He F, Wu B, 2022. Mechanism of effects of nickel or nickel compounds on intestinal mucosal barrier. Chemosphere 305(135429.

Hynes RO, 2009. The Extracellular Matrix: Not Just Pretty Fibrils. Science 326(5957): 1216-1219.

Jiang Z, Mu W, Yang Y, *et al.*, 2020. Cadmium exacerbates dextran sulfate sodium-induced chronic colitis and impairs intestinal barrier. Sci Total Environ 744(140844.

Kaphle B, Wang J, Ju J, *et al.*, 2024. Environmental risk assessment of the surface sediments based on trace elements analysis from the largest freshwater lake in the southern slope of the Himalaya, Nepal. Environ Monit Assess 197(1): 97.

Li H, Yu XH, Ou X, *et al.*, 2021. Hepatic cholesterol transport and its role in non-alcoholic fatty liver disease and atherosclerosis. Prog Lipid Res 83(101109.

Lu Changyuan LX, ZOU Xingli, CHENG Hongwei, XU Qian, 2015. Current situation and utilization technology of nickel ore in China. Chinese J Nature 37(4): 269-277.

Naryzhnaya NV, Maslov LN, Oeltgen PR, 2019. Pharmacology of mitochondrial permeability transition pore inhibitors. Drug Dev Res 80(8): 1013-1030.

Ringseis R, Gessner DK, Eder K, 2020. The Gut-Liver Axis in the Control of Energy Metabolism and Food Intake in Animals. Annu Rev Anim Biosci 8(295-319.

Sato R, 2020. Recent advances in regulating cholesterol and bile acid metabolism. Biosci Biotechnol Biochem 84(11): 2185-2192.

Sidhu P, Garg ML, Dhawan DK, 2005. Oxidative stress due to nickel toxicity in the liver of protein-deficient rats. Toxicol Mech Methods 15(6): 411-7.

Song X, Fiati Kenston SS, Kong L, *et al*., 2017. Molecular mechanisms of nickel induced neurotoxicity and chemoprevention. Toxicol 392(47-54.

Tammam AA-E, Khalaf AAA, Zaki AR, *et al*., 2022. Hesperidin protects rats' liver and kidney from oxidative damage and physiological disruption induced by nickel oxide nanoparticles. Front Physiol 13(912625.

Wang J, Bakker W, Zheng W, *et al*., 2022. Exposure to the mycotoxin deoxynivalenol reduces the transport of conjugated bile acids by intestinal Caco-2 cells. Arch Toxicol 96(5): 1473-1482.

Winter TA, 2006. The effects of undernutrition and refeeding on metabolism and digestive function. Curr Opin Clin Nutr Metab Care 9(5): 596-602.

Wu B, Cui H, Peng X, *et al*., 2013a. Dietary nickel chloride induces oxidative intestinal damage in broilers. Int J Environ Res Public Health 10(6): 2109-19.

Wu B, Cui H, Peng X, *et al*., 2013b. Dietary nickel chloride restrains the development of small intestine in broilers. Biol Trace Elem Res 155(2): 236-46.

Wu B, Cui H, Peng X, *et al*., 2014. Toxicological effects of dietary nickel chloride on intestinal microbiota. Ecotoxicol Environ Saf 109(70-6.

Wu B, Liu Y, Zhen J, *et al*., 2022. Protective effect of methionine on the intestinal oxidative stress and microbiota change induced by nickel. Ecotoxicol Environ Saf 244(114037.

Wu B, Liu Y, Zhen J, *et al*., 2022a. Protective effect of methionine on the intestinal oxidative stress and microbiota change induced by nickel. Ecotoxicol Environ Saf 244(114037.

Zhang Y, Ding X, Qiu H, *et al.* (2021) Correlation of nickel and arsenic levels in mid-pregnancy women with neonatal umbilical cord blood biomarkers. J Environ Hyg 11(3):230-236. https://doi.org/10.13421/j.cnki.hjwsxzz.2021.03.002

Zhou L, Chen SZ, Li YY, *et al*., 2025. Gut dysbiosis exacerbates intestinal absorption of cadmium and arsenic from contaminated rice in mice due to impaired intestinal barrier functions. Environ Sci Technol 59(7): 3459-3471.

Zou L, Su L, Sun Y, *et al*., 2017. Nickel sulfate induced apoptosis via activating ROS-dependent mitochondria and endoplasmic reticulum stress pathways in rat Leydig cells. Environ Toxicol 32(7): 1918-1926.